JACS
JOURNAL OF THE AMERICAN CHEMICAL SOCIETY

Article

pubs.acs.org/JACS

Tracking the Formation of a Polynuclear Co_{16} Complex and Its Elimination and Substitution Reactions by Mass Spectroscopy and Crystallography

Yue-Qiao Hu,[†] Ming-Hua Zeng,*[,†] Kun Zhang,[†] Sheng Hu,[‡] Fu-Fang Zhou,[†] and Mohamedally Kurmoo*[,§]

[†]Department of Chemistry and Chemical Engineering, Guangxi Normal University, Key Laboratory for the Chemistry and Molecular Engineering of Medicinal Resources (Ministry of Education), Guilin 541004, P. R. China

[‡]School of Chemical Engineering and Light Industry, Guangdong University of Technology, Guangzhou 510006, P. R. China

[§]Laboratoire DECOMET, Institut de Chimie de Strasbourg, Université de Strasbourg, CNRS-UMR 7177, 4 rue Blaise Pascal, CS 90032, 67081 Strasbourg Cedex, France

Supporting Information

ABSTRACT: We present the syntheses and structures of the biggest chiral cobalt coordination cluster, $[Co_{16}(L)_4(H_3L)_8(N_3)_6](NO_3)_2{\cdot}16H_2O{\cdot}2CH_3OH$ (**1**, where H_4L = *S*,*S*-1,2-bis-(1*H*-benzimidazol-2-yl)-1,2-ethanediol). **1** consists of two Co_4O_4 cubes ($Co_4(L)_2(H_3L)_2$) alternating with $Co_2(EO\text{-}N_3)_2Co_2$ ($Co_4(L)_2(H_3L)_2(N_3)_2$), bridged by the benzimidazole and azide nitrogen atoms to form a twisted ring. The ligand adopts both *cis* and *trans* forms, and all the rings have the same chiralilty. ESI-MS of **1** from a methanol solution of crystals reveals the fragment $[Co_{16}(L)_4(H_3L)_8(N_3)_6{+}2H]^{4+}$, suggesting the polynuclear core is stable in solution. ESI-MS measurements from the reaction solution found smaller fragments, $[Co_4(H_3L)_4{-}H]^{3+}$, $[Co_4(H_3L)_4{-}2H]^{2+}$, $[Co_4(H_3L)_4(N_3)_2]^{2+}$, and $[Co_2(H_3L)_2]^{2+}$, and ESI-MS from a methanol solution of the solid deposit found in addition the Co_{16} core. These results and the dependence on the synthesis time allow us to propose the process for the formation of **1**, which opens up a new way for the direct observation of the ligand-controlled assembly of clusters. In addition, the isolation of $[Co_4(H_3L)_4](NO_3)_4{\cdot}4H_2O$ (**2**) consisting of separate Co_4O_4 cubes with the ligands being only *cis* in crystalline form supports the proposal. Interestingly, N_3^- is replaced by either CH_3O^- or OH^-, and this is the first time that high-resolution ESI-MS is successfully utilized to examine both the step-by-step elimination and substitution of inner bridging ligands in such a high nuclear complex. Increasing the voltage results in stepwise elimination of azide from the parent cluster. The preliminary magnetic susceptibility of **1** indicates ferromagnetic cubes antiferromagnetically coupled to the squares within the cluster, though in a field of 2.5 kOe, weak and slow relaxation is observed below 4 K.

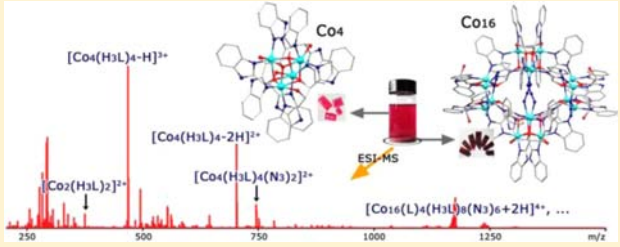

1. INTRODUCTION

Among the primary goals in chemistry is to understand bonding and the way reactions progress.[1−3] Although complex, there is now a clear understanding when dealing with small molecules. When the process involves big molecules, such as polyoxometalates (POMs),[4] supramolecular cages,[5,6] high-nuclear coordination molecules, etc.,[7] the problem becomes intractable. Techniques such as nuclear magnetic resonance (NMR) spectroscopy can provide information that allows researchers to follow certain events and propose a mechanism.[8] When it comes to proposing a process for formation of certain polynuclear metal−organic complexes, it has been difficult to do so for many years. Recently, electrospray ionization mass spectrometry (ESI-MS) has been used to study such formation, and several reports have appeared that follow cluster formation and also reactions.[9,10] ESI-MS is very useful when the metals are paramagnetic, rendering NMR difficult. We recently used the technique to demonstrate the existence and change of large magnetic clusters in solution, with a view toward processing them in solution for deposition on substrates.[11,12] In the present study we use it to work out the formation of a large cluster of $Co(II)_{16}$ in mixed methanol−water solvents.

We undertook this study in view of the recent attention that has been devoted to the design and synthesis of chiral polymetallic clusters of transition-metal ions.[13,14] Several different approaches for controlling the structure and properties of these clusters have been pursued.[14−18] However, only a few X-ray structurally characterized chiral high-nuclear-coordination molecular clusters of more than 10 metals are known, and their occurrences are often determined by serendipity rather than rational design.[19] The great difficulty is that most chiral aggregates usually crystallize as racemic mixtures or undergo rapid racemization in solution during the synthesis and coordination processing.[14,20]

Received: December 19, 2012
Published: May 7, 2013

   dx.doi.org/10.1021/ja3123784 | *J. Am. Chem. Soc.* 2013, 135, 7901−7908

To date, only 12 examples of cobalt-based polynuclear compounds are known with nuclearity ≥15 (Table S1). Up to now only three are Co_{16} clusters: $[Co_{16}(1,3\text{-bptb})_4(3,5\text{-bptpt})_4(OMe)_{12}(H_2O)_2]\cdot 25H_2O$,[21] comprising four linear $\{Co_4\}$ subunits; $[Co_{16}(BTC_4A)_4(\mu_4\text{-}Cl)_4(HCOO)_2(\mu\text{-}Mtta)_6(\mu\text{-}Mtta)_8]\cdot 10DMF\cdot 6CH_3CN\cdot 4Hdma$, stacked by wheel-like entities possessing four shuttlecock-like building blocks;[22] and $[Co_{16}(OH)_6(chp)_{22}(O_3PC_6H_9)_2(H_2O)_4]\cdot 10CH_2Cl_2\cdot 2H_2O$,[23] showing a distorted wheel of 10 sites, with the 6 remaining sites lying above and below the plane of the wheel. Our compound **1** represents the fourth member of the interesting Co_{16} family. Among more than 30 high-nuclearity (≥12) cobalt clusters, only one is non-centrosymmetric: the Co_{12} example, $\{(^tBu_3SiS)CoCl\}_{12}$. It crystallizes in the tetragonal system space group $P\bar{4}2_1c$, having a molecular wheel structure with ligand $SSi^tBu_3^-$.[24] To the best of our knowledge, the Co_{16} cluster, $[Co_{16}(bzimed)_4(H_3bzimed)_8(N_3)_6](NO_3)_2\cdot 16H_2O\cdot 2CH_3OH$ (**1**), presented in this work is the largest chiral cobalt cluster (Table S2 and CD spectra in Figure S1). Prior to our work, the largest cobalt cluster crystallizing in a chiral space group ($P2_12_12$) was a Co_7 example, $[Co^{II}_7(\mu_7\text{-}pzpz)_4Cl_2]$, with axial chirality resulting from the linear ligand N^2-(pyrazin-2-yl)-N^6-(6-(pyrazin-2-ylamino)pyridin-2-yl)pyridine-2,6-diamine.[25] Several Co_4 examples, such as $\{Na[Co_4L_3(OAc)_3](ClO_4)_{1.5}(H_2O)_{1.5}\}(ClO_4)(OH)_{0.5}\cdot 3H_2O$ with a flattened tetrahedral metal skeleton,[26] a Co_4O_4 cubane structure $[Co_4((R,R)\text{-}1\text{-}H)_4](ClO_4)_4\cdot 9EtOH$,[27a] and a quadruple helical structure $[Co_4[(R/S)\text{-}2\text{-}H]_4(dpp)_2](dpp)(ClO_4)\cdot 5MeOH$,[27b] have also been suggested and documented to the biggest chiral cobalt clusters, depending on the chiral ligands. In this context, Co_{16} is quite unique with its one-turn twist in a flat ring of single chirality and its high symmetry with the connections by the simple azide anion in its two different modes of coordination.

An important factor in the construction of such clusters is the choice of the "key" chiral ligand with stability of the enantiomeric form in the solvent and temperature range used, which will dictate not only the symmetry, topology, and number of metal ions but also the intramolecular and intermolecular interactions of the clusters.[11] Using enantiomerically pure ligands (*R* or *S* form) is the usual strategy for assembling chiral molecular clusters, which causes the compounds to crystallize in enantiomeric crystal forms.[15−18] Often short bridges, such as $OH^-/CH_3O^-/N_3^-$, have also been introduced because of their extremely versatile bridging modes in linking neighboring metal ions (μ_2, μ_3, μ_4, etc.) and their ability to stabilize clusters by mediating strong magnetic couplings between neighboring moment carriers.[11,12,28] Using this approach, we have been successful in creating several Co(II)-based single-molecule magnet complexes: a hydrogen-bonded dicubane Co_7 cluster coordinated by in situ solvothermally generated 1,2-bis(8-hydroxyquinolin-2-yl)-ethane-1,2-diol arranged in a trefoil,[29] and a series of cube-based triangular Co_{12} superclusters using the bulky ligand (1*H*-benzimidazol-2-yl)methanol.[30] In fact, the pre-design of high-nuclearity clusters with desired structures and properties remains a substantial challenge at this stage.[31] Recently, mass spectroscopy has grown into a powerful technique for discovering the complexity of inorganic supramolecular self-assembly in solution, and its effectiveness has also been proven in the case of cluster-based coordination systems.[6,9] In this context, one important aim was to explore the structures and properties of clusters in solution and solid state, with the hope that we can piece together the process of assembly, which may direct us in the synthesis of larger clusters.[9]

Herein, our choice of ligand is *S,S*-1,2-bis(1*H*-benzimidazol-2-yl)-1,2-ethanediol (*S,S*-H_4bzimed, H_4L; CD spectra are provided in Figure S1),[32] for the following reasons: (a) it has two optically active centers at the two ethane carbon atoms, (b) it exists as two geometrical isomers, *cis* and *trans* about the ethane C−C bond, (c) it can act as both acid and base with potentially up to seven charged states (2+ to 4−), (d) it can function as monodentate, bidentate, or tricap facial to one metal center as well as bridging to up to eight metals, and (e) it has the dimensions to stabilize up to three edges of a cube (Scheme S1).[27,32] Thus, the solvothermal reaction of $Co(NO_3)_2\cdot 6H_2O$, *S,S*-H_4bzimed, and NaN_3 in a 1:1 mixture of MeOH and water at 100 °C gives purple-red block crystals of $[Co_{16}(bzimed)_4(H_3bzimed)_8(N_3)_6](NO_3)_2\cdot 16H_2O\cdot 2CH_3OH$ (**1**) and $[Co_4(H_3bzimed)_4](NO_3)_4\cdot 4H_2O$ (**2**) from the filtrate (Figure S2). X-ray crystallographic, thermogravimetric (TG), and elemental analyses and ESI-MS confirm the formula. It is insoluble in water but is quite soluble in methanol and ethanol.

2. EXPERIMENTAL SECTION

2.1. Synthesis of the Compounds. *Synthesis of Complex* ***1*** *($[Co_{16}(bzimed)_4(H_3bzimed)_8(N_3)_6](NO_3)_2\cdot 16H_2O\cdot 2CH_3OH$).* A 1:1 mixture of MeOH and water (16 mL) containing $Co(NO_3)_2\cdot 6H_2O$ (291 mg, 1.0 mmol), *S,S*-H_4bzimed (294 mg, 1.0 mmol), NaN_3 (65 mg, 1 mmol), and triethylamine (0.3 mL) in a Teflon-lined steel bomb was heated at 100 °C for 1 day. The autoclave was then cooled at a rate of 10 °C·h^{-1}, and the purple-red crystals of **1** were collected, washed with H_2O, and dried in air (yield ca. 80% based on Co). Powder X-ray diffraction (PXRD), TG, IR, and elemental analyses (Figures S3 and S4) confirm the phase purity of the bulk product. Elemental analyses (%) calcd for **1**: C 44.37, H 3.71, N 18.30. Found: C 44.44, H 3.61, N 18.36. IR data for **1** (KBr, cm^{-1}): 3404(s), 2131(m), 2090(m), 1627(m), 1440(m), 1385(m), 1048(m), 741(m).

Synthesis of Complex ***2*** *($[Co_4(H_3bzimed)_4](NO_3)_4\cdot 4H_2O$).* At the end of the solvothermal synthesis and after filtering the crystals of **1**, the filtrate was allowed to evaporate in air, and after a few days few pink block single crystals were obtained in very low yield (<2%, Figure S2 right). The phase purity of this product was only confirmed by IR and elemental analyses because of the low yield. Elemental analyses (%) calcd for **2**: C 44.46, H 3.50, N 16.20. Found: C 44.50, H 3.61, N 16.35. IR data for **2** (KBr, cm^{-1}): 3425(s), 2353(m), 1623(m), 1455(m), 1385(m), 1110(m), 745(m).

2.2. X-ray Crystallography. Single-crystal X-ray diffraction (XRD) data collection for **1** was conducted on a Bruker SMART APEX II CCD diffractometer, and data for **2** were collected on an Oxford supernova diffractometer (Mo, λ = 0.71073 Å) by using the $\theta-\omega$ scan technique at 150 and 273 K, respectively. Raw frame data were integrated using SAINT[33] and corrected for absorption using SADABS.[34] The structures were solved by direct methods and refined with a full-matrix least-squares technique within the SHELXTL program package.[33] O9, O11, solvent H_2O molecules, and NO_3^- anion in **1** were refined isotropically; other non-hydrogen atoms were refined anisotropically. The hydrogen atoms were set in calculated positions and refined using the riding model. The crystallographic details are summarized in Table 1. Selected bond distances and bond angles are listed in Tables S3 and S4. Crystallographic data for the structural analyses have been deposited at the Cambridge Crystallographic Data Centre, reference numbers 915612 for **1** and 915611 for **2**. CIF files for two compounds can be found in the Supporting Information, or the crystallographic data can be obtained free of charge from the Cambridge Crystallographic Data Centre via http://www.ccdc.cam.ac.uk/data_request/cif.

2.3. Electrospray Ionization Mass Spectrometry. ESI-MS measurements were conducted at a capillary temperature of 275 °C. Aliquots of the solution were injected into the device at 0.3 mL/h. The

dx.doi.org/10.1021/ja3123784 | J. Am. Chem. Soc. 2013, 135, 7901−7908

Table 1. Crystal and Refinement Data for 1 and 2

	1	2
formula	$C_{194}H_{184}Co_{16}N_{68}O_{48}$	$C_{64}H_{60}Co_4N_{20}O_{24}$
formula weight	5178.89	1729.01
crystal system	orthorhombic	monoclinic
space group	$C222_1$	$C2$
T (K)	150(2)	293(2)
a (Å)	26.153(2)	17.5766(3)
b (Å)	29.754(2)	17.1387(2)
c (Å)	28.621(2)	12.8097(2)
α (deg)	90	90
β (deg)	90	95.836(2)
γ (deg)	90	90
V (Å^3)	22271(3)	3838.8(1)
D_c (g cm^{-3})	1.528	1.498
F(000)	10432	1763
Z	4	2
μ (mm^{-1})	1.245	0.938
reflns collected	60899	8912
unique reflns	21895	5916
R_{int}	0.0281	0.0168
data/parameters	21895/1444	5916/532
GOF	1.056	1.081
R_1, wR_2 [$I > 2\sigma(I)$]	0.0590, 0.1651	0.0347, 0.0931
R_1, wR_2 (all data)	0.0726, 0.1793	0.0395, 0.0981
Flack parameter	0.006(14)	−0.060(12)

mass spectrometer used for the measurements was a Thermo Exactive, and the data were collected in positive ion mode. The spectrometer was previously calibrated with the standard tune mix to give a precision of ca. 2 ppm in the region of 50−5000 m/z. The capillary voltage was 50 V, the tube lens voltage was 150 V, and the skimmer voltage was 25 V. The in-source energy was set to the range of 0−100 eV with a gas flow rate at 10% of the maximum.

2.4. Measurement Details. The reagents and solvents employed were commercially available and used as received without further purification. The C, H, and N microanalyses were carried out with a Vario Micro Cube elemental analyzer. The FT-IR spectra were recorded from KBr pellets containing ca. 0.5 mg of the compound in the range 4000−400 cm^{-1} on a Perkin-Elmer one FTIR spectrophotometer. PXRD intensities were measured at 293 K on a Rigaku D/max-IIIA diffractometer (Cu Kα, λ = 1.54056 Å). The crystalline powder samples were prepared by crushing the single crystals and scanned from 5 to 60° at a rate of 5°/min. Calculated patterns of **1** were generated by Diamond.[35] The thermal properties were measured using a gravimetric analyzer (Labsys evo TG-DSC/DTA) under a constant flow of dry nitrogen gas at a rate of 5 °C/min. Magnetization measurements were taken with a Quantum Design MPMS-XL7 SQUID instrument to 7 T for **1**. Data were corrected for the diamagnetism of the gelatin sample holder and the constituent atoms using Pascal's constants.

3. RESULTS AND DISCUSSION

3.1. Structural Analyses. X-ray structural analyses show that **1** crystallizes in the chiral orthorhombic space group $C222_1$ as discrete hexadecanuclear cation clusters with nitrate counterions. The asymmetric unit contains one-half of the formula unit, that is, eight Co(II) atoms, two fully deprotonated [*S*,*S*-bzimed]$^{4-}$ (mode A, *trans*- and μ_5), four singly deprotonated [*S*,*S*-H_3bzimed]$^-$ (mode B, *cis*- and μ_3; mode C, *cis*- and μ_2), three azide bridges (one end-to-end (EE) and two end-on (EO)), one nitrate counterion, and eight water and one methanol guest molecules (Figure 1). The unprecedented hexadecanuclear cation cobalt cluster can be described as two

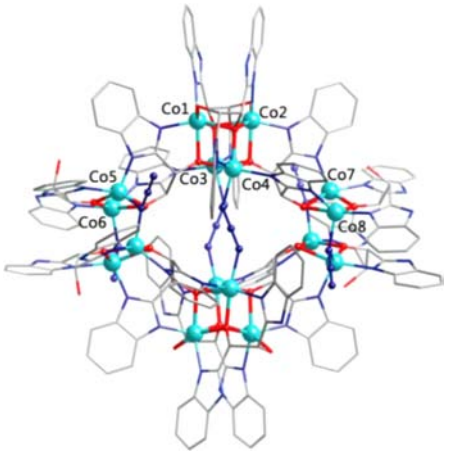

Figure 1. Structure of the integrated cation of **1**.

symmetrical cuboidal [Co_4O_4] tetramers and two double rhomboid [$Co_4O_4N_2$] tetramers, bound together by peripheral [*S*,*S*-bzimed]$^{4-}$ ligands (mode A) and central azide double-bridges, resulting in a giant metallamacrocycle. The maximum diameter of the [Co_{16}] cluster is about 25 Å, with a shortest intercluster center-to-center distance of about 18 Å (Figures S5−S7). As for the cuboidal [Co_4O_4] tetramer (Figure S8a), the four octahedral Co atoms lie at the vertices of a distorted cube, held together tightly by four μ_3-alkoxo oxygen atoms from two different [*S*,*S*-bzimed]$^{4-}$ ligands and two [*S*,*S*-H_3bzimed]$^-$ (mode B) ligands. In detail, Co1 and Co2 in distorted octahedral N_2O_4 environments are coordinated by two O,N-chelating sites, one μ_3-alkoxo oxygen atom and one monodentate alkoxo oxygen atom, while Co3 and Co4 both form distorted octahedral geometry $N_{EE}N_2O_3$ with three μ_3-alkoxo oxygen atoms and two nitrogen atoms from benzimidazole groups. The intracluster Co−O distances range from 2.048(4) to 2.251(4) Å, and the Co−O−Co angles range from 92.5(1) to 107.2(1)°. The intracube Co···Co distances are 3.018(1)−3.336(1) Å, which implies potential moderate magnetic interactions between the Co atoms. As for the double rhomboid [$Co_4O_4N_2$] tetramers (Figure S8b), two bipyramidal Co atoms linked by two O atoms form each Co_2O_2 rhomboid, which is connected by two EO azide bridges with Co−N distances of 2.029(6)−2.107(6) Å. The Co···Co distances in the rhomboid unit of 3.188(1)−3.361(1) Å are slightly longer than those in the [Co_4O_4] cube. On the other hand, the double imidazole bridges separating the [Co_4O_4] cube and the rhomboid tetramer unit with a distance of 5.730(1)−7.217(1) Å would transmit weak antiferromagnetic (AF) coupling between them.[36]

It is worth noting that the introduction of the *S*,*S*-H_4bzimed ligand containing rigid and flexible functional groups simultaneously with two chiral centers is critical for the formation of the hexadecanuclear cluster (Figure 2). The *S*,*S*-H_4bzimed ligand could be divided into two parts: the central *S*,*S*-1,2-bis-imidazolyl-1,2-ethanediol and the phenyl side rings. The former is responsible for bridging groups with chiral multidentate coordinated active atoms. Importantly, all the *S*,*S*-H_4bzimed ligands play key roles as chiral building units and maintain their chiral characteristics in the metal complex and high-temperature conditions, which are sterically demanding for the formation of the final chiral hexadecanuclear clusters. The phenyl ring offers additional aromatic interactions to influence the assembly and packing of the cluster structure.

dx.doi.org/10.1021/ja3123784 | J. Am. Chem. Soc. 2013, 135, 7901−7908

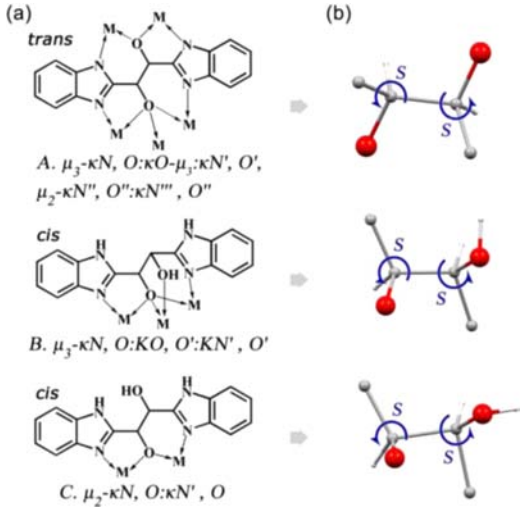

Figure 2. Coordination modes (a) and orientations of the chiral centers (b) for ligands in **1** and **2**.

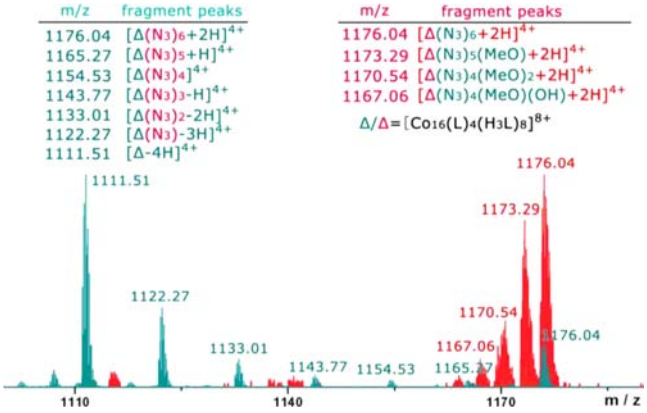

Figure 3. ESI-MS spectra of the crystals of **1** dissolved in MeOH. Red spectrum shows a substitution reaction of azide when the in-source energy is 0 eV. Green spectrum shows an elimination reaction of azide when the in-source energy is 40 eV.

Two phenyl side rings of the $[S,S\text{-}H_3bzimed]^-$ ligand make up one stacking pair and overlap each other in a face-to-face fashion. The center-to-center distance is 3.60 Å and the dihedral angle 12.2°, which indicates weak $\pi\cdots\pi$ interaction. The alignment and long separation between the phenyl rings of the $[S,S\text{-}H_3bzimed]^-$ ligands suggest that mutual repulsion and steric hindrance of the phenyl rings play vital roles in the formation of the hexadecanuclear cluster. The Co_{16} clusters are packed one next to the other along two directions in a manner without intercluster hydrogen interactions, although several hydrogen bonds exist between the solvent water molecules and the Co_{16} cations. Introduction of azide in the reaction mixture is important for binding the two types of tetramer to form the Co_{16} cluster. It adopts both bridging modes, EE between the two cubes of the Co_{16} cluster and EO within the rhomboid tetramer. On the other hand, the incorporation of azide templates between cuboidal $[Co_4O_4]$ tetramers and rhomboid $[Co_4O_4N_2]$ tetramers is more likely to induce core aggregation and highly desirable for magnetic exchange. **1** has a novel structure exhibiting cube-Co_4O_4 cyclic, bridged by *S,S*-H_4bzimed ligand and interlinked by N_3^- in the center of the cluster, which is a unique structure type, different from the well-known cyclic, cage-shaped, or disc-like molecular clusters.[31]

Interestingly, compared to some other 3d/3d-4f chiral polynuclear clusters with higher nuclearity (Table S5), for example, Mn_{22},[15] Fe_{28},[16] and Eu_{60},[17] the synthesis of the high-nuclearity chiral cobalt cluster is still in its infancy and remains a major challenge. Relative to other polynuclear cobalt clusters with nuclearities ≥15 comprising more than three kinds of different ligands, the cyclic-like Co_{16} cluster comprises only one bulky chelating/bridging ligand ($H_3bzimed^-$ and $bzimed^{4-}$), along with a small inner bridging ligand (EE and EO azide). Such a multimetallic coordination compound is an ideal candidate for utilizing the power of high-resolution ESI-MS to investigate and expand our understanding of the bottom-up self-assembly processes of inorganic complexes and supramolecular architectures, and cluster formation in solution (Table S6).[9]

3.2. Electrospray Ionization Mass Spectrometry. In order to probe the integrity of the cluster in solution and its behavior, crystals of **1** were dissolved in MeOH and probed by ESI-MS at 275 °C (Figures 3, S9, and S10).[11,12] The parent cluster ion was found at m/z 1176.04, which could be identified with isotopic envelopes corresponding to $[Co_{16}(L)_4(H_3L)_8(N_3)_6+2H]^{4+}$ (fit: 1176.04), here abbreviated as $[\Delta\text{-}(N_3)_6+2H]^{4+}$ ($\Delta = Co_{16}(L)_4(H_3L)_8$). It is formed by losing all the solvent molecules and two NO_3^-. When the in-source energy is 0 eV, some lower m/z value species are present at 1173.29, 1170.54, and 1167.06. These species could be assigned as follows: $[\Delta(N_3)_5(MeO)+2H]^{4+}$ (fit: 1173.29), $[\Delta\text{-}(N_3)_4(MeO)_2+2H]^{4+}$ (fit: 1170.54), $[\Delta(N_3)_4(MeO)\text{-}(OH)+2H]^{4+}$ (fit: 1167.06), which suggest that the N_3 bridges are sequentially replaced by MeO^- and OH^- (red spectrum in Figure 4, Table S7). This type of substitution was also observed for $[Co_7(L')_6(N_3)_6]_3\cdot 2ClO_4$ (L′ = 2-methoxy-6-[(methylimino)methyl]phenol), where μ_3-N_3^- was replaced by the higher affinity ligand CH_3O^-.[11] It is interesting to note that the bulkiness of the ligand H_4bzimed does not protect the N_3^- from replacement by either CH_3O^- or OH^-. On increasing the in-source energy stepwise to 20 eV the spectrum remains unchanged, but at 30 eV new weak peaks start to develop. At 40 eV these new peaks are prominent at m/z 1165.27, 1154.53, 1143.77, 1133.01, 1122.27, and 1111.51. They are assigned to the corresponding species $[\Delta(N_3)_5+H]^{4+}$, $[\Delta(N_3)_4]^{4+}$, $[\Delta\text{-}(N_3)_3-H]^{4+}$, $[\Delta(N_3)_2-2H]^{4+}$, $[\Delta(N_3)-3H]^{4+}$, and $[\Delta-4H]^{4+}$, indicating step-by-step elimination of the azide (blue spectrum in Figure 3, Table S8). Unfortunately, ESI-MS cannot differentiate between EE or EO N_3^- bridges. At higher energy the compound shows sign of degradation, and at 100 eV the spectrum is dominated by species of lower masses from decomposition products.

To the best of our knowledge, this is the first time that high-resolution ESI-MS is successfully utilized to examine the elimination and substitution of a bridging ligand such as N_3^- in a polynuclear complex.[11] The study of the chemistry of polynuclear complexes by mass spectroscopy is an important complement to ion exchange, template exchange, ligand exchange, supramolecular transformations, etc.[6,9] Furthermore, it is an excellent tool to demonstrate the existence and stability of clusters in solution and also provides important chemical information.[9]

In coordination chemistry, kinetic studies and crystallography provide a clear understanding of the fundamentals of the formation of mononuclear coordination complexes. There is less well-developed understanding of the processes of formation of larger clusters and those leading to metal−organic

dx.doi.org/10.1021/ja3123784 | J. Am. Chem. Soc. 2013, 135, 7901−7908

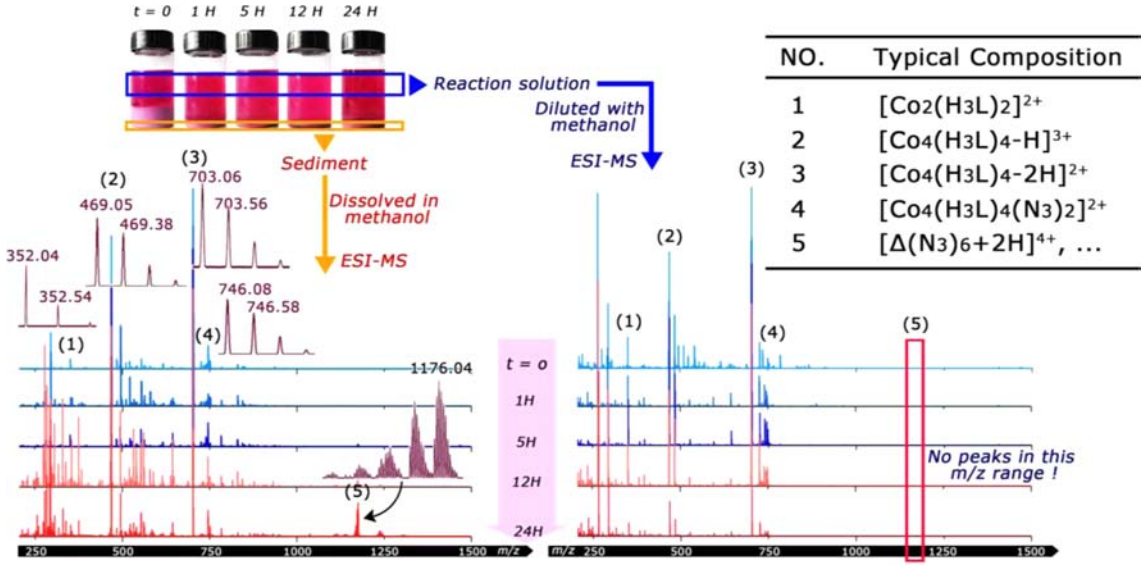

Figure 4. Experimental flow chart and mass spectrometry analysis of the assembly process of **1**. Note the presence of peak 5 corresponding to the Co_{16} cluster after 12 h from the solid (left) and its absence from solution under all conditions (right).

frameworks and coordination polymers.[9,10] The underlying problem is the large library of building blocks, fragments, and clusters potentially available as the number of building blocks increases. Mass spectroscopy is becoming a useful tool to develop our understanding of the polymerization process.[6,9] Therefore, in the present study we were able to identify several intermediates that are present in the Co_{16} cluster, in one case complemented by crystallographic results. Using these data, we propose a possible mechanism of self-assembly for the chiral clusters. This approach helped us to establish our synthetic method for high-nuclearity clusters, especially the synthesis of chiral clusters from chiral ligands.

The data shown in Figure 4 are derived from experiments on the five reaction products performed in the following way: The mixture of reactants was sufficiently stirred at room temperature for 20 h prior to solvothermal processing at 100 °C for different times, 0, 1, 5, 12, and 24 h. Following a period of sedimentation, two samples were extracted from each reaction, one of the solution and the other of the sediment; both were diluted/dissolved in methanol for ESI-MS measurements. Those from the solution are shown on the right of Figure 4, and those from the solid sediment are on the left.

In the preparation of the mixture for solvothermal reaction, the ligand and $Co(NO_3)_2{\cdot}6H_2O$ are dissolved in the methanol−water solvent followed by sodium azide and triethylamine after 15 min. This results in a heavy pink precipitate that is reduced in quantity as the reaction time is increased. The sediment (a mixture of crystals and powders) is easily dissolved in methanol but is insoluble in water. The latter may be due to the fact that the hydrophobicity of the peripheral ligands protects the cluster from the water. In contrast, the ligand is highly soluble in methanol and prevents Co_{16} from crystallizing. Thus, a compromise of a mixture of water−methanol yields good-quality crystals of the Co_{16} cluster. The content of this mixture can be used to control the crystallization process, which was useful in our ESI-MS study.

An important observation was that the species present in the solutions are also present in the sediments, indicating that the fragments forming the solid exist in solution, and it is thus possible to follow the reaction and provide a mechanism for the formation of the high-nuclearity cluster.

The spectra can be fully assigned on the basis of m/z values and isotopic distributions to identify all major peaks (Figure 4, Table S9). Importantly, the most prominent peaks, m/z 469.05 and 703.06, can be unambiguously assigned to the $[Co_4(H_3L)_4-H]^{3+}$ and $[Co_4(H_3L)_4-2H]^{2+}$ cores, which is supported by the crystallographic observation of a cubane structure $Co_4(H_3bzimed)_4(NO_3)_4$ (**2**). In addition, several low-intensity peaks can be assigned to $[Co_2(H_3L)_2]^{2+}$ at m/z 352.04 (fit: 352.04) and $[Co_4(H_3L)_4(N_3)_2]^{2+}$ at m/z 746.08 (fit: 746.08). The presence of these simple cluster fragments indicates that *S,S*-H_4bzimed is a versatile polydentate ligand and it readily forms these conventional small structures prior to further formation of giant clusters. It is worth noting that the intensity of peaks of fragments containing N_3^- groups, such as $[Co_4(H_3L)_4(N_3)_2]^{2+}$, are very low, and their formation is an important rate-determining step which is useful to us in observing the self-assembly process.

The spectrum recorded after the reaction mixture had been heated for 1 h can be seen to have changed little compared with the previous one. For longer reaction times, the species populating the m/z range of 200−1000 do not change significantly, while numerous peaks corresponding to a range of substitution species of $[Co_{16}]$ cluster are present at the mass range of >1000, with the peaks' intensities increasing with time (Figures 4 and 5). It is important to note that the reactant-related peaks of unchanged intensity and final product species of increased intensity are correlated, and the reactant-related species possibly perform as the intermediates in this reaction.

Through assigning the fragment ions observed in the ESI mass spectra of the reaction solution of **1**, and by noting the changes in intensity of prominent peaks with time (Figure 5 left), we were able to propose that the assembly of Co_{16} supercluster occurs through the formation of $[Co_4L_4]$ species (i.e., $[Co_4(H_3L)_4-H]^{3+}$ (m/z 469.05) and $[Co_4(H_3L)_4-2H]^{2+}$ (m/z 703.06)) which are similar to the $[Co_4O_4]$ unit of the Co_{16} cluster and the most prominent peaks in the spectrum recorded. We then followed the small, stable fragment ions containing two cobalt ions and two ligands, $[Co_2(H_3L)_2]^{2+}$ ($m/$

dx.doi.org/10.1021/ja3123784 | J. Am. Chem. Soc. 2013, 135, 7901−7908

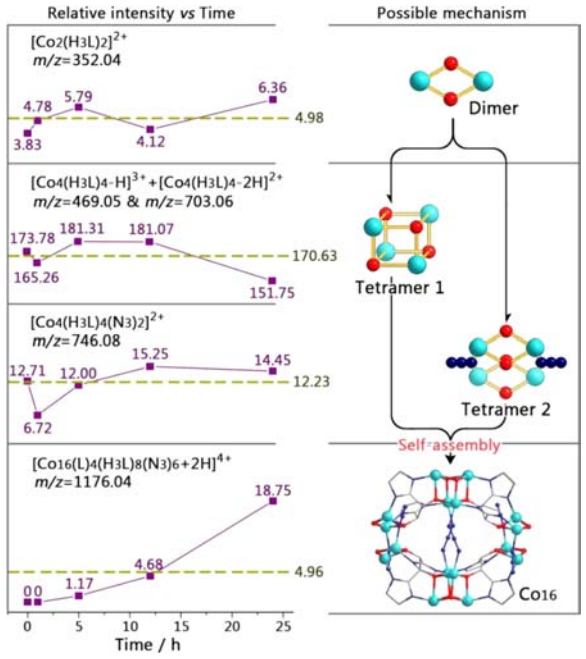

Figure 5. Left: Plots of relative peak intensity versus time of reactant-related fragment ions and the Co_{16} fragment ions. The yellow dashed lines of average intensity values are shown as a guide to help us understand the general trends of changes in peak intensity over time. Right: Schematic diagram of a possible mechanism of the formation process of Co_{16}. The structures tetramer 1 and Co_{16} are based on crystallographic data, and dimer and tetramer 2 are fragments of the structure of Co_{16}.

z 352.04), which were subsequently linked via the N_3^- ligand to form the $[Co_4L_4(N_3)_2]$ species $[Co_4(H_3L)_4(N_3)_2]^{2+}$ (m/z 746.08), which is similar to the $[Co_4O_4N_2]$ unit and further combined with $[Co_4L_4]$ unit to form the final Co_{16} cluster, $[Co_{16}(L)_4(H_3L)_8(N_3)_6{+}2H]^{4+}$ (m/z 1176.04). Additionally, the reactant-related peaks for $[Co_4(H_3L)_4{-}H]^{3+}$ (m/z 469.05), $[Co_4(H_3L)_4{-}2H]^{2+}$ (m/z 703.06), and $[Co_4(H_3L)_4(N_3)_2]^{2+}$ (m/z 746.08) were of unchanged intensity during the course of the actual MS studies. They confirm that the $[Co_4L_4]$ and $[Co_4L_4(N_3)_2]$ species are equilibrium-stable intermediates of the Co_{16} supercluster formation mechanism (Figure 5 right). It is important to note that the small clusters Co_2 and Co_4 are formed in the solid at the early stages, while the large cluster Co_{16} only starts forming at 12 h reaction time and the quantity increases by 24 h. In contrast, the small clusters are present in all solutions, but the larger cluster is absent in some. This observation suggests that the large cluster crystallizes favorably in the methanol–water mixture.

At the end of the solvothermal synthesis and after filtering the crystals of **1**, the filtrate was allowed to evaporate in air, and after several days few pink block crystals of a second phase, $[Co_4(H_3bzimed)_4](NO_3)_4{\cdot}4H_2O$ (**2**), were obtained. A single crystal was selected for X-ray data collection. The structure was found to belong to the monoclinic system and the chiral space group C_2. It is constructed of a similar cuboidal Co_4O_4 tetramer unit but without the azide and with only four of the $H_3bzimed^-$ ligands (mode B) around it (Figure S11). Interestingly, the ligands are all in the *cis*-form, and each is coordinated to the metal ions along three edges of the cube. Each cobalt atom is hexacoordinated by four oxygen atoms and two nitrogen atoms. Each ligand is deprotonated only at one alcohol site, which then adopts the μ_3-mode while the other acts as a terminal OH. To avoid steric hindrance of the phenyl rings, the ligands are arranged in parallel pairs, each pair on opposite faces of the cube. The phenyl rings are face-to-face with adjacent clusters and thus provide the weak $\pi{-}\pi$ interaction. Importantly, the difference between the structures Co_{16} ring and Co_4 cube is the geometrical form of the ligands, being both *cis* and *trans* in the former and charged 1− and 4−, respectively, while it is only *cis* and 1− in the latter. The two clusters are stable in methanol solution. Isolation of the Co_4 cluster from the solution (m/z 469.05 and 703.06) is an indication that it is an integral component in the building of the bigger Co_{16} cluster, in agreement with the ESI-MS results (Figure S12, Table S10).

The ESI (CSI)-MS technique has been applied in the research field of supramolecular assembly for several years, and greatly developed by the groups of Stang,[6] Fujita,[5a] Cronin,[9] and others. Comparing to POMs and supramolecular cages, there is still a lack of good examples to study the assembly mechanism of high nuclear cluster compounds prepared by solvothermal reaction. The above results are significant since it is a typical example to bridge the gap between solid-state and solution studies, so that the mechanism of self-assembly can be explored in a more systematic way.[10] Previous studies have done very well with the identification of the clusters under study to demonstrate their stability and integrity.[9] In a few cases, exchange of ions has been shown to take place.[37] Our study adds another two steps in this progress where we were able to demonstrate the exchange of coordinating ligand (azide to methoxide and hydroxide) and furthermore, the sequential elimination of azide.[11] We also show that by studying both the solution and the solid products of a reaction as a function of time important information can be obtained to piece together a mechanism, or identification of a species which can then be crystallized for XRD, as is the case with compound **2**.

3.3. Magnetic Properties. Magnetic susceptibility data for **1** were collected over the temperature range of 2–300 K under an applied field of 1000 Oe (Figure 6). The $\chi_m T$ value for **1** is

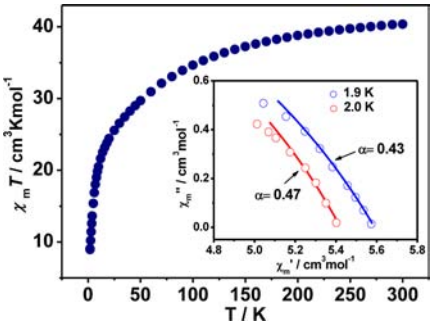

Figure 6. $\chi_m T$ vs T in the temperature range of 2–300 K, and (inset) Cole–Cole plots of the ac susceptibilities for **1**.

40.36 $cm^3{\cdot}K/mol$ at 300 K, which is much larger than the value expected for 16 isolated spin-only $S = 3/2$ Co(II) ions (30 $cm^3{\cdot}K/mol$ assuming $S = 3/2$ and $g = 2.0$), indicating significant orbital contributions of the octahedral Co(II) ions.[29,30] The reciprocal molar magnetic susceptibility plotted versus temperature obeys the Curie–Weiss law above 100 K, with C = 44.2(3) $cm^3{\cdot}K/mol$ (2.712 per Co(II) ions) and $\theta = -26.8(1)$ K (Figure S13). The Curie constant is as expected for octahedral Co(II). The negative Weiss constant is slightly more negative than the value expected for an isolated octahedral Co(II) due to the effect of spin–orbit coupling, suggesting that

dx.doi.org/10.1021/ja3123784 | J. Am. Chem. Soc. 2013, 135, 7901–7908

the intracluster coupling may be weakly AF. As the temperature is lowered, the $\chi_m T$ value of **1** decreases gradually to 8.95 $cm^3 \cdot K/mol$ at 2.0 K.

The field dependence of the magnetization at 2.0 K increases progressively to 21.6 $N\beta$ at 7 T. The value is much lower than that expected for 16 paramagnetic Co(II), 38.4 $N\beta$ assuming 2.4 $N\beta$ per Co(II). This is also consistent with the temperature dependence of $\chi_m T$ value at low temperatures and confirms that interaction between the Co(II) ions is AF.

The magnetic susceptibilities of cobalt complexes are complicated by significant orbital effects, and it is hard to predict the magnetic behavior in such high-nuclearity and less symmetric systems, since the dependence of the J values on the Co−O−Co angle is not obvious.[30,38] When the values reported for different cobalt(II) clusters are compared, some general observations can be made. It is noted that several kinds of magnetic pathways can be considered: one is that within Co_4O_4 (J_1) and $Co_4O_4N_2$ units (J_2 and J_3), the other is between units (J_4 and J_5) (Scheme S2, Tables S11 and S12). From previous findings,[39] we know that ferromagnetic (F) coupling between neighbors is observed for the cube structure (J_1), the edge-sharing Co_2O_2 pair (J_2), and the Co_2-EO-N_3 bridge (J_3).[40] However, it is AF for coupling through the benzimidazole (J_4) and the Co_2-EE-N_3 bridges (J_5). Assuming these are the same in the Co_{16} cluster, we will then have four F tetramers AF coupled to one another. The overall expected ground state has zero moment. Given the large local anisotropy of the cobalt(II) and the weak interactions that are involved, it is very difficult to predict the final state and the complicated and subtle balance at finite temperatures.

To probe the relaxation properties, the temperature-dependent ac magnetic susceptibilities in the temperature range of 1.8−10 K were collected in 2.5 Oe ac field oscillating at frequencies in the range of 1−997 Hz and a bias of 2500 Oe dc field. Figure S14 shows the in-phase (χ_m') and out-of-phase signals (χ_m'') versus T. These showed frequency-dependent out-of-phase signals below 3 K, which may be attributed to superparamagnetism.[11,29,30]

At fixed temperatures of 1.9 and 2.0 K, the Cole−Cole plots of χ'' versus χ' displays part of a semicircle, which can be fitted by a generalized Debye model with α parameters of 0.43 and 0.47, respectively (Figure 6, inset). The data are rather limited for a more thorough analysis.

4. CONCLUSION

In conclusion, the identification of several stable fragments of the structure of $[Co_{16}(bzimed)_4(H_3bzimed)_8(N_3)_6](NO_3)_2 \cdot 16H_2O \cdot 2CH_3OH$ in the ESI-MS spectra from two complementary systems, both reaction mother liquor and solid sediment, as a function of time allowed us to piece together a proposal for the process of its formation. Isolation and X-ray analysis of $[Co_4(H_3bzimed)_4](NO_3)_4 \cdot 4H_2O$ gave confidence to the proposal. More interestingly, this is the first time that high-resolution ESI-MS is successfully utilized to examine the step-by-step elimination and substitution of the inner N_3^- bridges by either CH_3O^- or OH^- within a Co_{16} cluster. For a Co_4 cube structure, as the intracluster bridge μ_3-O-CH_2 is part of the bulky ligand $H_3bzimed^-$, a phenomenon similar to that observed with the azide bridge is hindered. These studies show that with judicious choice of appropriate molecular building blocks and conditions that closely mirrors the crystallization conditions, mass spectroscopy provides a better definition of the boundary between "designed" and "serendipitous" assembly of complex and high-nuclearity species. The magnetic susceptibility of the former suggests a superparamagnetic behavior.

■ ASSOCIATED CONTENT

Supporting Information

Crystal data in CIF files and additional TG, PXRD, magnetism, and ESI-MS data. This material is available free of charge via the Internet at http://pubs.acs.org.

■ AUTHOR INFORMATION

Corresponding Author

zmh@mailbox.gxnu.edu.cn; kurmoo@unistra.fr

Notes

The authors declare no competing financial interest.

■ ACKNOWLEDGMENTS

This work was supported by NSFC (No. 91022015, 91122032), GXNSFC (2010GXNSFF013001), Guangxi Province Science Funds for Distinguished Young Scientists ((2012GXNSFFA060001), and the Project of Talents Highland of Guangxi Province, as well as the Project of Talents Highland of Colleges and Universities in Guangxi Province. S.H. thanks the NSFC (No. 21001030), and M.K. thanks the CNRS-France for funding.

■ REFERENCES

(1) Pauling, L. *The nature of the chemical bond*, 3rd ed.; Cornell University Press: Ithaca, NY, 1960.

(2) Yin, Z.; Wang, Q. X.; Zeng, M. H. *J. Am. Chem. Soc.* **2012**, *134*, 4857.

(3) Chen, X. M.; Tong, M. L. *Acc. Chem. Res.* **2007**, *40*, 162.

(4) Pasparakis, G.; Krasnogor, N.; Cronin, L.; Davis, B. G.; Alexander, C. *Chem. Soc. Rev.* **2010**, *39*, 286.

(5) (a) Fujita, M.; Tominaga, M.; Hori, A.; Therrien, B. *Acc. Chem. Res.* **2005**, *38*, 371. (b) Pluth, M. D.; Bergman, R. G.; Raymond, K. N. *Acc. Chem. Res.* **2009**, *42*, 1650. (c) Koblenz, T. S.; Wassenaar, J.; Reek, J. N. H. *Chem. Soc. Rev.* **2008**, *37*, 247.

(6) Chakrabarty, R.; Mukherjee, P. S.; Stang, P. J. *Chem. Rev.* **2011**, *111*, 6810.

(7) Fujita, M.; Powell, A.; Creutz, C. *From the Molecular to the Nanoscale: Synthesis, Structure, and Properties*; Elsevier Ltd.: Oxford, UK, 2004; Vol. 7.

(8) Spiess, H. W. *Overview of NMR of Bulk Polymers. NMR Spectroscopy of Polymers: Innovative Strategies for Complex Macromolecules*; ACS Symposium Series; American Chemical Society: Washington, DC, 2011; Chapter 2, p 17.

(9) Miras, H. N.; Wilson, E. F.; Cronin, L. *Chem. Commun.* **2009**, 1297.

(10) (a) Xu, F.; Miras, H. N.; Scullion, R. A.; Long, D. L.; Thiel, J.; Cronin, L. *Proc. Natl. Acad. Sci. U.S.A.* **2012**, *109*, 11609. (b) Newton, G. N.; Onuki, T.; Shiga, T.; Noguchi, M.; Matsumoto, T.; Mathieson, J. S.; Nihei, M.; Nakano, M.; Cronin, L.; Oshio, H. *Angew. Chem., Int. Ed.* **2011**, *50*, 4844. (c) Seeber, G.; Cooper, G. J. T.; Newton, G. N.; Rosnes, M. H.; Long, D. L.; Kariuki, B. M.; Kögerler, P.; Cronin, L. *Chem. Sci.* **2010**, *1*, 62. (d) Sun, Q. F.; Murase, T.; Sato, S.; Fujita, M. *Angew. Chem., Int. Ed.* **2011**, *50*, 10318. (e) Fujita, D.; Takahashi, A.; Sato, S.; Fujita, M. *J. Am. Chem. Soc.* **2011**, *133*, 13317. (f) Cui, F. J.; Li, S. G.; Jia, C. D.; Mathieson, J. S.; Cronin, L.; Yang, X. J.; Wu, B. *Inorg. Chem.* **2012**, *51*, 179.

(11) (a) Zhou, Y. L.; Zeng, M. H.; Wei, L. Q.; Li, B. W.; Kurmoo, M. *Chem. Mater.* **2010**, *22*, 4295. (b) Wei, L. Q.; Zhang, K.; Feng, Y. C.; Wang, Y. H.; Zeng, M. H.; Kurmoo, M. *Inorg. Chem.* **2011**, *50*, 7274.

(12) (a) Chen, Q.; Zeng, M. H.; Wei, L. Q.; Kurmoo, M. *Chem. Mater.* **2010**, *22*, 4328. (b) Zhou, Y. L.; Zeng, M. H.; Liu, X. C.; Liang, H.; Kurmoo, M. *Chem.—Eur. J.* **2011**, *17*, 14084. (c) Zhang, K.; Dai,

J.; Wang, Y. H.; Zeng, M. H.; Kurmoo, M. *Dalton Trans.* **2013**, *42*, 5439.
(13) Hof, F.; Craig, S. L.; Nuckolls, C.; Rebek, J., Jr. *Angew. Chem., Int. Ed.* **2002**, *41*, 1488.
(14) Xuan, W. M.; Zhu, C. F.; Liu, Y.; Cui, Y. *Chem. Soc. Rev.* **2012**, *41*, 1677.
(15) Liu, C. M.; Xiong, R. G.; Zhang, D. Q.; Zhu, D. B. *J. Am. Chem. Soc.* **2010**, *132*, 4044.
(16) Zhang, Z. M.; Li, Y. G.; Yao, S.; Wang, E. B.; Wang, Y. H.; Clérac, R. *Angew. Chem., Int. Ed.* **2009**, *48*, 1581.
(17) Kong, X. J.; Wu, Y. L.; Long, L. S.; Zheng, L. S.; Zheng, Z. P. *J. Am. Chem. Soc.* **2009**, *131*, 6918.
(18) (a) Kato, N.; Mita, T.; Kanai, M.; Therrien, B.; Kawano, M.; Yamaguchi, K.; Danjo, H.; Sei, Y.; Sato, A.; Furusho, S.; Shibasaki, M. *J. Am. Chem. Soc.* **2006**, *128*, 6768. (b) Bozoklu, G.; Gateau, C.; Imbert, D.; Pécaut, J.; Robeyns, K.; Filinchuk, Y.; Memon, F.; Muller, G.; Mazzanti, M. *J. Am. Chem. Soc.* **2012**, *134*, 8372.
(19) Kong, X. J.; Long, L. S.; Zheng, Z. P.; Huang, R. B.; Zheng, L. S. *Acc. Chem. Res.* **2010**, *43*, 201.
(20) Wang, C.; Zhang, T.; Lin, W. B. *Chem. Rev.* **2012**, *122*, 1084.
(21) Lin, W. Q.; Leng, J. D.; Tong, M. L. *Chem. Commun.* **2012**, *48*, 4477.
(22) Xiong, K.; Jiang, F. L.; Gai, Y. L.; He, Z. Z.; Yuan, D. Q.; Chen, L.; Su, K. Z.; Hong, M. C. *Cryst. Growth Des.* **2012**, *12*, 3335.
(23) Ma, Y. S.; Song, Y.; Tang, X. Y.; Yuan, R. X. *Dalton Trans.* **2010**, *39*, 6262.
(24) Sydora, O. L.; Wolczanski, P. T.; Lobkovsky, E. B.; Rumberger, E.; Hendrickson, D. N. *Chem. Commun.* **2004**, 650.
(25) Wang, W. Z.; Ismayilov, R. H.; Lee, G. H.; Liu, I. P. C.; Yeh, C. Y.; Peng, S. M. *Dalton Trans.* **2007**, 830.
(26) Li, Y. M.; Xiang, S. C.; Sheng, T. L.; Zhang, J. J.; Hu, S. M.; Fu, R. B.; Huang, X. H.; Wu, X. T. *Inorg. Chem.* **2006**, *45*, 6577.
(27) (a) Isele, K.; Gigon, F.; Williams, A. F.; Bernardinelli, G.; Decurtins, S. *Dalton Trans.* **2007**, 332. (b) Deville, C.; Spyratou, A.; Aguirre-Etcheverry, P.; Besnard, C.; Williams, A. F. *Inorg. Chem.* **2012**, *51*, 8667. (c) Zhou, Y. L.; Meng, F. Y.; Zhang, J.; Zeng, M. H.; Liang, H. *Cryst. Growth Des.* **2009**, *9*, 1402.
(28) Weng, D. F.; Wang, Z. M.; Gao, S. *Chem. Soc. Rev.* **2011**, *40*, 3157.
(29) Chen, Q.; Zeng, M. H.; Zhou, Y. L.; Zou, H. H.; Kurmoo, M. *Chem. Mater.* **2010**, *22*, 2114.
(30) Zeng, M. H.; Yao, M. X.; Liang, H.; Zhang, W. X.; Chen, X. M. *Angew. Chem., Int. Ed.* **2007**, *46*, 1832.
(31) (a) Murrie, M. *Chem. Soc. Rev.* **2010**, *39*, 1986. (b) Kostakis, G. E.; Perlepes, S. P.; Blatov, V. A.; Proserpio, D. M.; Powell, A. K. *Chem. Rev.* **2012**, *256*, 1246. (c) Nakano, M.; Oshio, H. *Chem. Soc. Rev.* **2011**, *40*, 3239. (d) Timco, G. A.; Faust, T. B.; Tuna, F.; Winpenny, R. E. P. *Chem. Soc. Rev.* **2011**, *40*, 3067.
(32) Isele, K.; Broughton, V.; Matthews, C. J.; Williams, A. F.; Bernardinelli, G.; Franz, P.; Decurtins, S. *Dalton Trans.* **2002**, 3899.
(33) *SHELXTL*, version 6.10; Bruker Analytical Instrumentation: Madison, WI, 2000.
(34) Sheldrick, G. M. *SADABS*, version 2.05; University of Götingen: Götingen, Germany.
(35) Brandenburg, K. *DIAMOND*, version 3.2i; Crystal Impact GbR: Bonn, Germany.
(36) Tian, Y. Q.; Cai, C. X.; Ren, X. M.; Duan, C. Y.; Xu, Y.; Gao, S.; You, X. Z. *Chem.—Eur. J.* **2003**, *9*, 5673.
(37) (a) Newton, G. N.; Cooper, G. J. T.; Kögerler, P.; Long, D. L.; Cronin, L. *J. Am. Chem. Soc.* **2008**, *130*, 790. (b) Xu, F.; Scullion, R. A.; Yan, J.; Miras, H. N.; Busche, C.; Scandurra, A.; Pignataro, B.; Long, D. L.; Cronin, L. *J. Am. Chem. Soc.* **2011**, *133*, 4684.
(38) Langley, S.; Helliwell, M.; Sessoli, R.; Teat, S. J.; Winpenny, R. E. P. *Inorg. Chem.* **2008**, *47*, 497.
(39) (a) Tong, M. L.; Monfort, M.; Juan, J. M. C.; Chen, X. M.; Bu, X. H.; Ohba, M.; Kitagawa, S. *Chem. Commun.* **2005**, 233. (b) Zhou, Y. L.; Wu, M. C.; Zeng, M. H.; Liang, H. *Inorg. Chem.* **2009**, *48*, 10146.
(40) Kurmoo, M. *Chem. Soc. Rev.* **2009**, *38*, 1353.